

Anechoic Chamber Evaluation Using the Matrix Pencil Method

Benoît Fourestié, Zwi Altman, *Senior Member, IEEE*, and Motohisa Kanda, *Fellow, IEEE*

Abstract—A new method for evaluation of an anechoic chamber using the matrix pencil method is presented. A signal measured between two antennas placed in an anechoic chamber is sliced into small frequency intervals and is processed using the matrix pencil method. In each interval, the measured signal is decomposed into its propagating-wave components, which correspond to a direct propagation between two antennas and reflected propagating waves from absorbing walls. The ratio of amplitudes of the reflected wave components with respect to the direct path propagation gives a new measure of quality factor for an anechoic chamber.

Index Terms— Absorber, anechoic chamber, matrix pencil method.

I. INTRODUCTION

MICROWAVE anechoic chambers are currently in use for a variety of indoor antenna measurements, electromagnetic interference (EMI) measurements, and electromagnetic compatibility (EMC) measurements. The prime requirement is that a transmitting antenna at one location within a chamber generates a known field throughout a volume of the chamber, which has dimensions sufficient to perform antenna measurements. This volume is frequently called a “quiet zone” and the level of reflected waves within it determines the performance of the anechoic chamber.

A typical anechoic chamber is shown in side view in Fig. 1. Pyramidal horns or open-ended waveguides (OEG's) are used as transmitting antennas with their apertures inside the plane of the absorber points on the chamber wall. The net power delivered to the transmitting antenna is the difference between the incident power P_{inc} and reflected power P_{refl} as measured with a calibrated directional coupler (four ports) with calibrated power meters.

Electromagnetic field measurements in an anechoic chamber are usually performed in the near-field region of a transmitting standard antenna. The approach used to establish the standard field involves calculating the radiated field intensity in the near-field region of the transmitting antenna. The antenna typically used for the anechoic chamber measurements consist of a series of open-ended waveguides at frequencies below 450 MHz and a series of rectangular pyramidal horns above 450 MHz.

Manuscript received June 15, 1998; revised April 5, 1999.
B. Fourestié and Z. Altman are with CNET, France Télécom, 92794 Issy Les Moulineaux Cedex 9, France.
M. Kanda is with the National Institute of Standards and Technology, Boulder, CO 80303 USA.
Publisher Item Identifier S 0018-9375(99)06713-7.

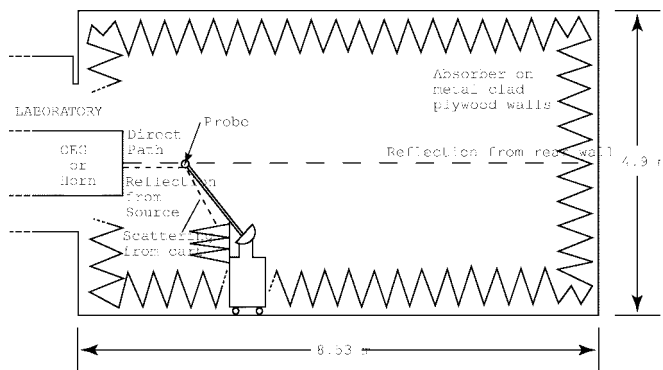


Fig. 1. A side view of the NIST anechoic chamber.

The failure of an anechoic chamber to provide a truly free-space test environment affects the measurement accuracy. The performance of a rectangular RF anechoic chamber has been typically checked by measuring the relative insertion loss versus separation distance between a source antenna and a receiving antenna [1].

The parameter $S_{21}(f)$ is the ratio of the outgoing power wave at the receiving antenna to the incident power wave at the transmitting antenna [2]. Therefore, antenna insertion loss $|S_{21}|^2$ is the ratio of power delivered to the receiving antenna or probe to the input power of the transmitting antenna. If the anechoic chamber is a perfect free-space simulator, the relative insertion loss between two polarization-matched antennas varies with distance according to the Friis transmission formula [3]

$$|S_{21}|^2 = P_r/P_t = G_r G_t (\lambda/4\pi d)^2 \quad (1)$$

where P_t is the net power delivered to the transmitting antenna, P_r is the power received by the receiving antenna, G_t is the near-field gain of the transmitting antenna, G_r is the near-field gain of the receiving antenna, d is the distance between the two antennas, and λ is the wavelength. Experimental data are compared with the calculated free-space transmission loss using appropriate near-field transmitting antenna gains. Disagreement between the measured and calculated transmission loss is a measure of reflection from chamber surfaces. Field strength plotted in Fig. 2 as a function of distance from the horn shows standing waves resulting from chamber reflections [1].

The purpose of this paper is to present a new anechoic chamber evaluation technique using the matrix pencil method [4]. The measurement strategy is as follows. A system consisting of a transmitting and a receiving antenna is placed in an anechoic

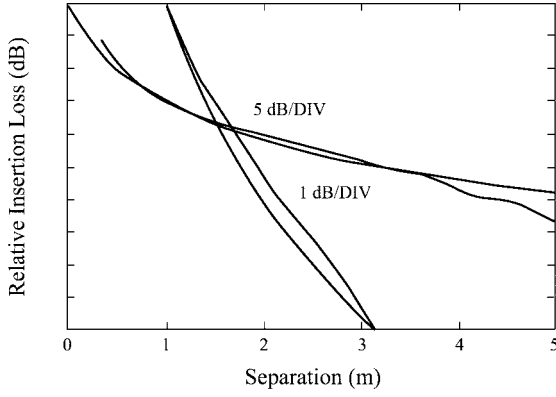


Fig. 2. Relative insertion loss between source and probe antenna versus separation distance with free-space transmission loss curve fitted at 1 m: frequency = 175 MHz: OEG source antenna.

chamber. The S -parameters of the system are measured by use of a vector network analyzer in both amplitude and phase to obtain the complex 2×2 S matrix. The system is perfectly reciprocal; hence $S_{21} = S_{12}$. The measured complex signal of S_{21} is sliced into small frequency intervals and is decomposed into a small number of complex exponential functions by using the matrix pencil method. The resultant exponential functions are processed in order to identify the terms corresponding to the different propagation components, i.e., the direct wave between the transmitting antenna and the receiving antenna, and the contingent reflected wave components from anechoic chamber walls. To verify whether the propagating components are related to chamber resonance or to antenna mismatch, we apply the decomposition into propagating components on S_{11} and S_{22} parameters on the same frequency intervals as S_{21} . In this case, the propagating components are guided components due to mismatching between the cable and the antenna and between the antenna and free-space. Ideally, S_{11} and S_{22} should be independent of the positions of the antennas in the chamber. If resonance or reflections occur in the chamber, the decomposition of S_{11} and S_{22} into complex exponential functions will vary with antenna position or polarization. Thus, the analysis of S_{11} and S_{22} using the matrix pencil method in conjunction with that of S_{21} allows us to isolate the influence of the measurement test site.

Once the reflected propagating components have been identified, the performance (a measure of quality factor) of an anechoic chamber is determined by the comparison of the amplitudes of the reflected wave components with respect to the direct wave component. We have previously used the matrix pencil method in the frequency domain to correlate measurements in semi-anechoic and anechoic chambers at resonance-free frequency ranges [5]. It is complementary to the time-domain approaches that we have pursued previously [6]–[8]. In these measurements, the wide-band time-domain reflectometer was used to evaluate the bistatic performance of the scattering coefficients of RF/microwave absorbers. In the time-domain measurements, windowing can be used as a clutter-reduction tool to separate out the desired signal. The matrix pencil method used in the frequency-domain analysis is thought to be more robust to noise [4]. Moreover, the required measurement devices are less elaborate.

II. MATRIX PENCIL METHOD—A REVIEW

Consider a complex function S which represents S_{21} , S_{11} or S_{22} . We model this function as a sum of complex exponentials

$$S(f) = \sum_{i=1}^M a_i \exp(\gamma_i f). \quad (2)$$

The function $S(f)$ is sampled at N frequency points $f_k = k\Delta f$, $k = 0, 1, \dots, N-1$

$$S(k) = \sum_{i=1}^M a_i \exp(\gamma_i k\Delta f). \quad (3)$$

The problem now reduces to finding the best estimates for a_i and γ_i , $i = 1, \dots, M$. This problem can be solved in various ways. Prony's method [9] and the matrix pencil method [4] are among the most common techniques.

The matrix pencil method is conceptually more efficient and more robust to noise [4] and is thus used here. Let $z_i = \exp(\gamma_i \Delta f)$, then $S(k) = \sum_{i=1}^M a_i z_i^k$ which can be written as the product

$$S(k) = [z_1^p z_2^p \dots z_m^p] \begin{bmatrix} a_1 & & & 0 \\ & a_2 & & \\ & & \ddots & \\ 0 & & & a_m \end{bmatrix} \begin{bmatrix} z_1^{k-p} \\ z_2^{k-p} \\ \vdots \\ z_m^{k-p} \end{bmatrix} \quad (4)$$

$p \in (0, \dots, k).$

The passage from the k th sample to the $k+1$ th sample can be carried out by multiplying (4) by a diagonal matrix having z_i in its diagonal

$$S(k+1) = [z_1^p z_2^p \dots z_m^p] \begin{bmatrix} a_1 & & & 0 \\ & a_2 & & \\ & & \ddots & \\ 0 & & & a_m \end{bmatrix} \cdot \begin{bmatrix} z_1 & & & 0 \\ & z_2 & & \\ & & \ddots & \\ 0 & & & z_m \end{bmatrix} \begin{bmatrix} z_1^{k-p} \\ z_2^{k-p} \\ \vdots \\ z_m^{k-p} \end{bmatrix} \quad (5)$$

$p \in (0, \dots, k).$

Define two matrices Y_1 and Y_2

$$[Y_1] = \begin{bmatrix} S(0) & S(1) & \dots & S(L-1) \\ S(1) & S(2) & & S(L) \\ \vdots & \vdots & & \vdots \\ S(N-L-1) & S(N-L) & & S(N-2) \end{bmatrix} \quad (6)$$

$$[Y_2] = \begin{bmatrix} S(1) & S(2) & \dots & S(L) \\ S(2) & S(3) & & S(L+1) \\ \vdots & \vdots & & \vdots \\ S(N-L) & S(N-L+1) & & S(N-1) \end{bmatrix}. \quad (7)$$

Using (4) and (5), we can write the above two matrices as follows:

$$[Y_1] = [Z_1][A][Z_2] \quad (8)$$

$$[Y_2] = [Z_1][A][Z_0][Z_2] \quad (9)$$

where

$$[Z_1] = \begin{bmatrix} 1 & 1 & \cdots & 1 \\ z_1 & z_2 & \cdots & z_M \\ \vdots & \vdots & \ddots & \vdots \\ z_1^{N-L-1} & z_2^{N-L-1} & \cdots & z_M^{N-L-1} \end{bmatrix} \quad (10)$$

$$[Z_2] = \begin{bmatrix} 1 & z_1 & \cdots & z_1^{L-1} \\ 1 & z_2 & \cdots & z_2^{L-1} \\ \vdots & \vdots & \ddots & \vdots \\ 1 & z_M & \cdots & z_M^{L-1} \end{bmatrix} \quad (11)$$

$$[Z_0] = \begin{bmatrix} z_1 & & & 0 \\ & z_2 & & \\ & & \ddots & \\ 0 & & & z_M \end{bmatrix} \quad (12)$$

$$[A] = \begin{bmatrix} a_1 & & & 0 \\ & a_2 & & \\ & & \ddots & \\ 0 & & & a_M \end{bmatrix}. \quad (13)$$

Next, consider the matrix pencil

$$[Y_2] - z[Y_1] = [Z_1][A]([Z_0] - zI)[Z_2] \quad (14)$$

where I is the identity matrix. From (14) we can see that if both $N - L \geq M$ and $L \geq M$, the matrix pencil $[Y_2] - z[Y_1]$ is of rank M , unless $z = z_i$, $i = 1, 2, \dots, M$ and then the rank is $M - 1$. In this case, the z_i 's are the eigenvalues of the matrix equation

$$[Y_2][\nu_i] = z_i[Y_1][\nu_i] \quad (15)$$

where $[\nu_i]$ is the eigenvector corresponding to z_i . Using the Moore–Penrose pseudo-inverse $[Y_1]^+$ of $[Y_1]$ [10], we can find z_i from the eigenvalue equation

$$\left\{ [Y_1]^+[Y_2] - z_i[I] \right\} [\nu_i] = [0] \quad (16)$$

where $[Y_1]^+$ can be calculated via the SVD or using the formula

$$[Y_1]^+ = \left([Y_1]^H [Y_1] \right)^{-1} [Y_1]^H. \quad (17)$$

In presence of noise, the choice of $L = N/2$ gives optimal results [11]. Once the z_i 's are known, the coefficient amplitudes a_i are easily solved from the least-square problem

$$\begin{bmatrix} S(0) \\ S(1) \\ \vdots \\ S(N-1) \end{bmatrix} = \begin{bmatrix} 1 & 1 & \cdots & 1 \\ z_1 & z_2 & \cdots & z_M \\ \vdots & \vdots & \ddots & \vdots \\ z_1^{N-1} & z_2^{N-1} & \cdots & z_M^{N-1} \end{bmatrix} \begin{bmatrix} a_1 \\ a_2 \\ \vdots \\ a_M \end{bmatrix}. \quad (18)$$

III. ANALYSIS

Consider a system consisting of two log-periodic antennas facing each other in an anechoic chamber. The complex S parameters of the system are measured as a function of frequency using a vector network analyzer. The network analyzer was calibrated at the antenna ports. The measured signal was sampled uniformly and the matrix pencil was applied directly to the measured data.

In order to physically identify the propagating components of the measured signal, we decompose $S_{21}(f)$ into a sum of complex exponentials

$$S_{21}(f) = \sum_{i=1}^M a_i \exp(\gamma_i f) \quad (19)$$

where γ_i 's are complex constants of the form $\gamma_i = \alpha_i + j\beta_i$. The α_i 's are damping factors that take into account the attenuation due to propagation, reflections, and antenna factors. β_i has the dimension of radians-seconds and is related to the propagation time of the i th component between the two antennas. The product $\beta_i f$ is related to the phase accumulation due to the propagation between the two antennas and for the direct propagating component ($i = 1$) we have

$$\varphi_1 = \beta_1 f = \frac{2\pi d}{c} f \bmod(2\pi) = 2\pi t_1 f \bmod(2\pi) \quad (20)$$

where t_1 is the time needed for the direct propagating component to travel a distance d between the two antennas at the velocity of light in free-space c . The reflected components include both a phase term due to propagation and a term due to reflections on the anechoic chamber walls.

The coefficients a_i and γ_i can be derived by sampling $S_{21}(f)$ uniformly at frequencies f_k , $f_k = k\Delta f$ and applying the matrix pencil method to the sampled signal. Here the entire frequency range has been divided into subintervals with a width corresponding to a phase cycle of the direct component. The number of complex exponentials required to accurately decompose the signal over each subinterval is derived using a cutoff criterion in the singular value decomposition (SVD) routine used by the matrix pencil algorithm [4]. The cutoff criterion is determined by a threshold ε

$$\frac{\sigma_i}{\sigma_{\max}} \leq \varepsilon \quad (21)$$

where σ_i is the singular value under consideration and σ_{\max} the highest singular value. The threshold ε defines the upper limit for the error introduced by the SVD reconstruction. The value of ε is inversely proportional to the signal-to-noise ratio (SNR) of the measurements. SNR values of 25 to 30 dB can be easily achieved with the experimental setup and the value of -30 dB has been chosen for ε throughout this work.

The analyses of $S_{11}(f)$ and $S_{22}(f)$ are carried out in addition to that of $S_{21}(f)$ to ensure that the resonances identified using $S_{21}(f)$ correspond to the chamber influence and not to antenna mismatch. Antenna mismatch is polarization independent; thus, propagating components varying with the polarization highlight chamber-related resonances. The $S_{11}(f)$ and $S_{22}(f)$ decompositions are carried out on the same frequency intervals as $S_{21}(f)$ and using the same

cutoff criterion in the SVD. The resonance in the chamber can modify $S_{11}(f)$ and $S_{22}(f)$ in a way depending on the positions of the antennas and, therefore, both of these parameters are processed.

IV. RESULTS

We have used two identical log-periodic antennas for the anechoic chamber evaluation and a vector network analyzer for S -parameter measurements. The vector network analyzer was calibrated with reference planes at the antenna input terminals. The anechoic chamber shown in Fig. 1 is constructed within a metal-shielded room approximately 4.9 m high \times 6.7 m wide \times 8.5 m long. It is lined with RF absorbing materials on the interior walls, ceiling, and floor to reduce electromagnetic reflections. The absorber used is a commercially available carbon-impregnated fire-retardant urethane foam with pyramid points.

The S -parameter measurements between two identical log-periodic antennas placed in the anechoic chamber were performed from 200 to 600 MHz using a vector network analyzer with a 1 MHz step. The S -parameter measurements were performed for both horizontal and vertical polarizations of the log-periodic antennas, facing each other, polarization-matched, at a distance of 3 m. The data were decomposed over frequency intervals (windows) of 25 MHz. Thus, each window contained 25 uniformly distributed samples. The coefficients a_i and γ_i in (19) were calculated using the matrix pencil method. In each 25-MHz subinterval, $S_{21}(f)$ is approximated by a sum of complex exponentials, which represent the direct propagation between the two log-periodic antennas and the reflected wave components from the anechoic chamber walls. In frequency intervals where resonance or parasitic reflections occur, a greater number of complex exponentials are found.

Fig. 3 shows the amplitude and Fig. 4 the phase of $S_{21}(f)$ for antennas separated by a distance of 3 m in horizontal polarization. The period in Fig. 3 grows slowly with frequency. This behavior is explained by the fact that the guided and free-space paths between the active regions of the two log-periodic antennas become longer as frequency decreases. Fig. 5 shows the values of the β_i 's and Fig. 6 the magnitude of the transmission coefficients a_i for the horizontal polarization. Each β_i and a_i value in the figures is attributed to the central frequency of the corresponding 25-MHz window. The uncertainty of the frequency location of the resonances is thus of the order of half the window bandwidth. Fig. 6 shows a significant reflected wave, 30% (2.3 dB) relative to the direct component at about 270 MHz. A more significant reflection was observed at about 230 MHz. The magnitude of the reflected wave becomes as large as the direct wave component. This phenomenon at 230 MHz may be related to the anechoic chamber resonance. The insertion-loss measurement between a standard-gain antenna and a probe antenna also indicated this very similar result at 229 MHz [1]. When the theoretical inverse-square curve was fitted to the measurement curves as given in (1), a maximum difference range of -0.6 to 0.6 dB along the boresight axis of the standard gain antenna was observed at 229 MHz.

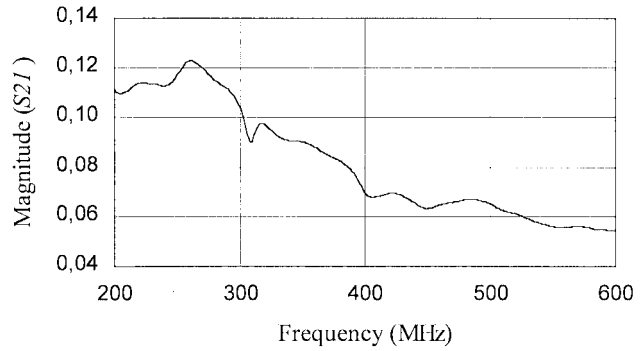


Fig. 3. The amplitude of $S_{21}(f)$ for the horizontal polarization.

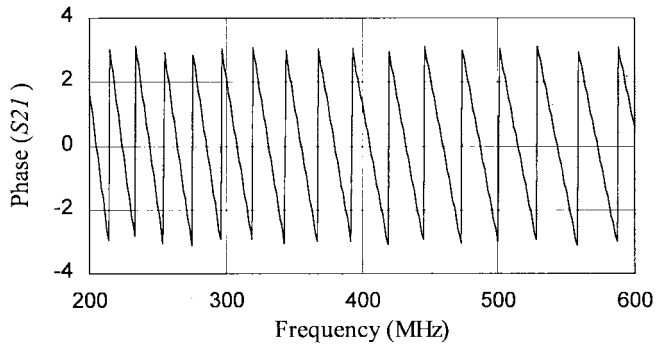


Fig. 4. The phase of $S_{21}(f)$ for the horizontal polarization.

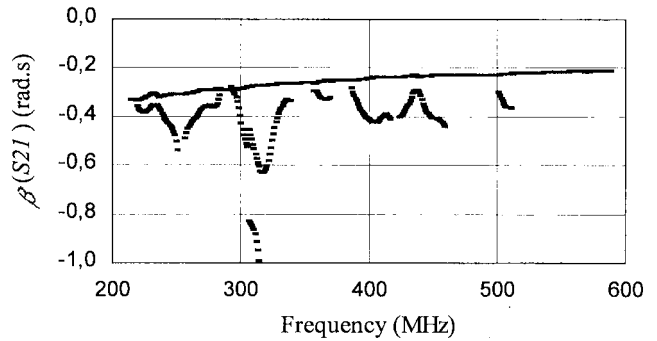


Fig. 5. The β_i 's for $S_{21}(f)$ for the horizontal polarization.

Fig. 7 shows the amplitude and Fig. 8 the phase of $S_{21}(f)$

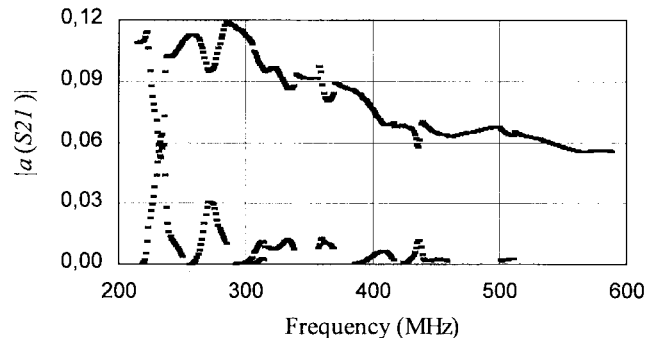
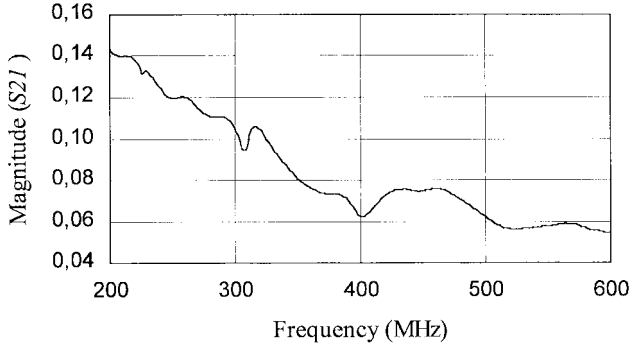
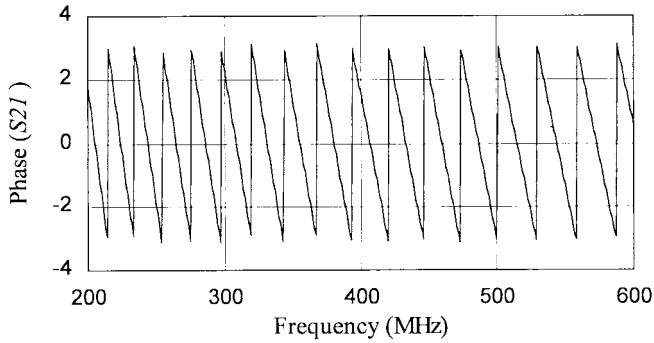
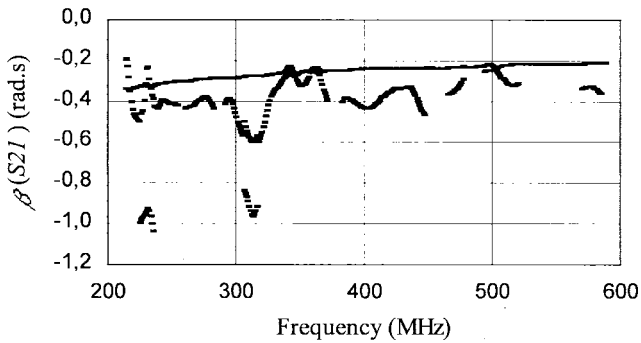
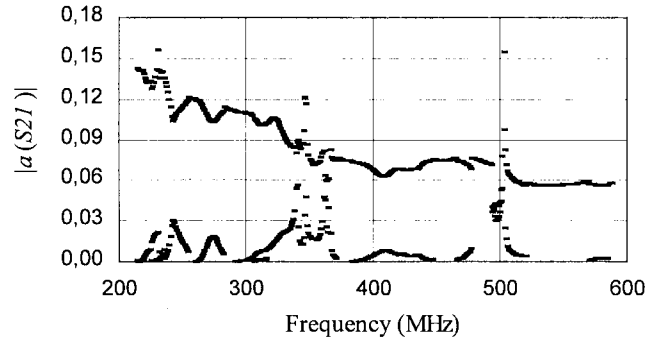
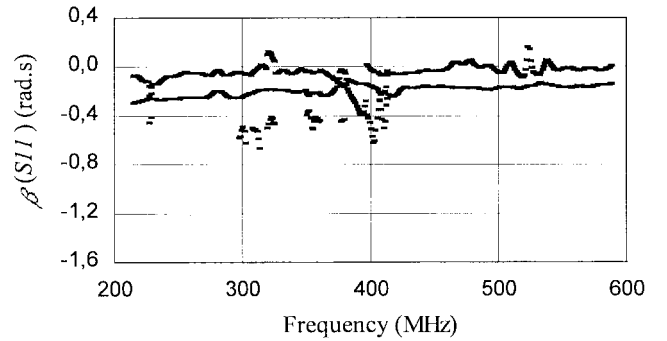
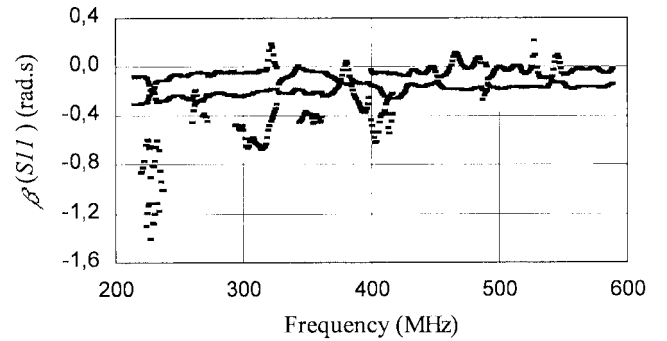


Fig. 6. The magnitude of the transmission coefficients α_i 's for $S_{21}(f)$ for the horizontal polarization.

Fig. 7. The amplitude of $S_{21}(f)$ for the vertical polarization.Fig. 8. The phase of $S_{21}(f)$ for the vertical polarization.Fig. 9. The β_i 's for $S_{21}(f)$ for the vertical polarization.

for the vertical polarization. Fig. 9 shows the β_i 's and Fig. 10 the α_i 's for the vertical polarization. We have noticed clear reflection components at around 230, 270, 350, and 500 MHz. This 230-MHz reflection is very consistent with the horizontal result, which may be related to the chamber resonance.

To discriminate between reflections intrinsic to the antennas and reflections due to the test site, similar decompositions were carried out on $S_{11}(f)$ and $S_{22}(f)$. Fig. 11 shows the β_i 's of the reflection coefficient $S_{11}(f)$ for horizontal and Fig. 12 for the vertical polarization. Additional exponential terms appear in the decomposition for the vertical polarization between 220 and 235 MHz. These terms depend on the antennas locations and highlight the resonance phenomena occurring at these frequencies. Although less important, the same behavior is

Fig. 10. The magnitude of the transmission coefficients α_i 's for $S_{21}(f)$ for the vertical polarization.Fig. 11. The β_i 's for $S_{11}(f)$ for the horizontal polarization.Fig. 12. The β_i 's for $S_{11}(f)$ for the vertical polarization.

observed around 270 MHz. Similar results were obtained with the decomposition of $S_{22}(f)$.

Vertical polarization is generally more sensitive than horizontal polarization in identifying certain chamber imperfections such as an antenna mast, transmitting and receiving cables, and other obstructions that might adversely affect measurements.

V. CONCLUSION

This paper described a new systematic measurement technique for the evaluation of an RF anechoic chamber using the matrix pencil method. It is based on a decomposition of the measured signal into its propagating components in the form of complex exponential functions over selected frequency intervals. The proposed method has successfully characterized

anechoic chamber imperfections due to poor performance of RF absorbing material, other parasitic reflections and coupling effects.

The proposed method has several attractive features: no *a priori* knowledge of the system, such as antenna factors or system configuration, is needed. The algorithm requires very little computational resources. Unlike techniques based on Fourier transform of data sampled in the frequency domain, relatively narrow-band signals can be handled adequately. Furthermore, its requirements in terms of frequency-sampling step size remain low.

REFERENCES

- [1] D. A. Hill, M. Kanda, E. B. Larsen, G. H. Koepke, and R. D. Orr, "Generating standard reference electromagnetic fields in the NIST anechoic chamber, 0.2 to 40 GHz," *Nat. Inst. Stand. Technol. Tech. Note* 1335, Mar. 1990.
- [2] K. Kurokawa "Power waves and scattering matrix," *IEEE Trans. Microwave Theory Tech.*, vol. MTT-13, pp. 194–202, Mar. 1965.
- [3] H. T. Friis, "A note on simple transmission formula," *Proc. IRE*, vol. 24, pp. 254–256, May 1946.
- [4] T. K. Sarkar and O. Pereira, "Using the matrix pencil method to estimate the parameters of a sum of complex exponentials," *IEEE Antennas Propagat. Mag.*, vol. 37, pp. 48–55, Feb. 1995.
- [5] B. Fourestié, Z. Altman, J. Wiat, and A. Azoulay, "On the use of the matrix pencil method to correlate measurements at different test sites," *IEEE Trans. Antennas Propagat.*, to be published.
- [6] R. R. Delyzer, C. L. Holloway, R. T. Johnk, A. R. Ondrejka, and M. Kanda, "A new measure of quality factor for low-frequency anechoic chamber based on absorber reflection coefficients," *IEEE Trans. Electromagn. Compat.*, vol. 38, pp. 576–584, Nov. 1996.
- [7] R. T. Johnk, A. R. Ondrejka, S. Tofani, and M. Kanda, "Time-domain measurements of the electromagnetic backscatter of pyramidal absorbers and metallic plates," *IEEE Trans. Electromagn. Compat.*, vol. 35, pp. 429–433, Nov. 1993.
- [8] S. Tofani, A. R. Ondrejka, M. Kanda, and D. A. Hill, "Bistatic scattering of absorbing materials from 30 to 1000 MHz," *IEEE Trans. Electromagn. Compat.*, vol. 34, pp. 304–307, Aug. 1992.
- [9] R. Prony, "Essai expérimental et analytique sur les lois de la dilatabilité de fluides élastiques et sur celles de la force expansive de la vapeur de l'alcool à différentes températures," *Paris J. L'Ecole Polytechnique*, vol. 1, pp. 24–76, 1795.
- [10] G. H. Golub and C. F. Van Loan, *Matrix Computation*. Baltimore, MD: Johns Hopkins Univ. Press, 1989.
- [11] Y. Hua and T. K. Sarkar, "Generalized pencil-of-function method for extracting poles of an EM system from its transient response," *IEEE Trans. Antennas Propagat.*, vol. 37, pp. 229–234, Feb. 1989.



Benoît Fourestié was born in Paris, France, in 1975. He received the Telecommunication Engineering degree from the Institut National des Télécommunications, Evry, France, in 1997 and the D.E.A. degree in digital telecommunication systems from L'Ecole Nationale Supérieure des Télécommunications, Paris, France, in 1997. He is currently working toward the Ph.D. degree in electrical engineering at CNET—National Center of Telecommunication Studies of France Telecom, Issy Les Moulineaux, France.

His research interests include antenna measurements, near-field measurements, electromagnetic compatibility, and digital signal processing.



Zwi Altman (S'88–M'90–SM'98) received the B.Sc. and M.Sc. degrees in electrical engineering from the Technion-Israel Institute of Technology, Haifa, in 1986 and 1989, respectively, and the Ph.D. degree in electronics from the Institut National Polytechnique de Toulouse, France, in 1994.

He was a "Lauréat de la Bourse LAVOISIER" of the French Foreign Ministry in 1994 and from 1994 to 1996 he was a Postdoctoral Research Fellow in the Electromagnetic Communication Laboratory, Electrical Engineering Department, University of Illinois, Urbana. In 1996 he joined the CNET-National Center of Telecommunication Studies of France Telecom, Issy Les Moulineaux, France. His research interests include electromagnetic compatibility, bio-electromagnetics, antenna measurements, computational electromagnetics and signal processing.

Dr. Altman is currently an Associate Editor for the IEEE TRANSACTIONS ON ELECTROMAGNETIC COMPATIBILITY.



Motohisa Kanda (S'67–M'78–SM'83–F'88) received the B.S.E.E. degree from Keio University, Tokyo, Japan, and the M.S.E.E. and Ph.D. degrees from the University of Colorado, Boulder, in 1966, 1968, and 1971, respectively.

From 1965 to 1966, he was a Research Technician at Keio University, where he did research on the avalanche breakdown in the germanium p-n junction at a cryogenic temperature. From 1966 to 1971 he was a Research Assistant at the University of Colorado, where he conducted research on impact ionization of impurities in *n*-type germanium and nonreciprocal behavior in a solid-state plasma at millimeter and submillimeter wavelengths. In 1971 he joined the staff of the Electromagnetic Fields Division, the National Institute of Standards and Technology (formerly Bureau of Standards), Boulder, CO, where he is currently the Leader of the Fields and Interference Metrology Group. Concurrently, he serves as a Professor Adjoint in the Electrical and Computer Engineering Department, University of Colorado, Boulder.

Dr. Kanda is Editor-in-Chief of the IEEE TRANSACTIONS ON ELECTROMAGNETIC COMPATIBILITY. He was Chairman of the U.S. Commission A of the International Union of Radio Science (URSI) from 1990 to 1993 and was elected to serve as Vice Chairman of the International Commission A of URSI from 1994 to 1996. He has received the Bronze Medal (1981 and 1992) and Silver Medal (1989) from the U.S. Department of Commerce. He has received three IEEE Electromagnetic Compatibility (EMC) Transaction Best Paper Awards in 1982, 1989, and 1992, and other numerous awards from the IEEE EMC Society and the Department of Commerce.